JOURNAL OF PROPULSION AND POWER
Vol. 17, No. 4, July–August 2001

Triple Langmuir Probe Measurements in the Plume of a Pulsed Plasma Thruster

Robert Eckman,* Lawrence Byrne,† and Nikolaos A. Gatsonis‡
Worcester Polytechnic Institute, Worcester, Massachusetts 01609
and
Eric J. Pencil§
NASA John H. Glenn Research Center at Lewis Field, Cleveland, Ohio 44135

An experimental apparatus using triple langmuir probes was designed to obtain electron temperature and density in the plume of a laboratory-model pulsed plasma thruster (PPT) operating at discharge energy levels of 5, 20, and 40 J. Electron temperature and density were obtained on two planes parallel and perpendicular to the thruster electrodes passing through the thruster's centerline. Measurements were obtained for radial distances of 6, 10, 12, 14, 16, 18, and 20 cm and for polar angles of 10, 20, 30, and 45 deg with respect to the center of the Teflon® propellant face. Plume properties show large angular variation on the perpendicular to the electrodes plane but small variation on the parallel plane confirming the asymmetry of the PPT plume. Electron density and temperature decrease with increasing radial distance from the Teflon surface. The average maximum temperature is between 2 and 4 eV for all discharge energy levels considered. The average maximum electron density is 1.6×10^{20}, 1.6×10^{21}, and 1.8×10^{21} m^{-3} for the 5-, 20-, and 40-J discharge. The time-average electron density increases with increasing discharge energy and is in the range between 10^{19} and 2×10^{20} m^{-3} for 5 J, 3×10^{19} and 10^{21} m^{-3} for 20 J, and 5×10^{19} and 1.4×10^{21} m^{-3} for 40 J.

Nomenclature

A_n	=	area of probe $n = 1, 2, 3$
d_s	=	probe sheath thickness
e	=	electron charge
J_i	=	ion current density
J_{i0}	=	random ion thermal current density
Kn_{st}	=	Knudsen number for s–t collisions
k	=	Boltzmann constant
L_p	=	probe length
$m_{i(e)}$	=	mass of ion (electron)
$N_e^*(r, \theta)$	=	average maximum electron density
$\langle N_e \rangle(r, \theta)$	=	time-average electron density
$n_e(r, \theta, t; i)$	=	electron density of the ith sample
$n_e^{\max}(r, \theta)$	=	maximum electron density during a pulse
r	=	radial distance downstream from the center of Teflon® surface
r_p	=	probe radius
s	=	probe spacing
$T_e(r, \theta, t; i)$	=	electron temperature of the ith sample
$T_e^{\max}(r, \theta)$	=	maximum electron temperature
$T_e^*(r, \theta)$	=	average maximum temperature
$\langle T_e \rangle(r, \theta)$	=	time-average temperature
T_i	=	ion temperature
t	=	time
U_i	=	ion speed
V_{dn}	=	voltage difference between probes 1 and $n = 2, 3$
V_f	=	floating potential
Z_i	=	number charge of ion i
β	=	parameter that characterizes variation of ion current with probe potential
ε_0	=	permittivity of free space
η	=	nondimensional B
θ	=	polar angle measured from the center of the Teflon® surface
λ_D	=	Debye length
λ_{st}	=	mean free path for collisions between species s and t
τ_L	=	end-effect parameter
χ	=	nondimensional potential at a probe

Received 4 March 2000; revision received 28 August 2000; accepted for publication 8 February 2001.

*Space Grant Fellow and Graduate Research Assistant, Mechanical Engineering Department, 100 Institute Road; currently Systems and Performance Engineer, General Electric Aircraft Engines, 1000 Western Avenue, Lynn, MA 01910. Student Member AIAA.

†Space Grant Fellow and Graduate Research Assistant, Mechanical Engineering Department, 100 Institute Road. Student Member AIAA.

‡Associate Professor, Mechanical Engineering Department, 100 Institute Road. Senior Member AIAA.

§Aerospace Engineer, On-Board Power and Propulsion. Member AIAA.

Introduction

A PULSED plasma thruster (PPT) is a type of electromagnetic propulsion system that ablates, ionizes, and then accelerates a solid Teflon® propellant to generate thrust. This type of thruster has been investigated since the 1960s and has been flown successfully several times in the past.[1,2] Interest, and consequently research, in PPTs has been renewed in the past half decade due to their specific impulses in excess of 1000 s, low-power requirements, simple propellant management, and the success of initial flight tests.[3]

Successful integration of PPTs on spacecraft requires the comprehensive evaluation of possible plume/spacecraft interactions. The PPT plume consists of neutrals and ions from the decomposition of the Teflon propellant and material from electrode erosion, as well as electromagnetic fields and optical emissions. The overall goal of this research program is to develop a predictive ability of the PPT plume environment and to assess potential plume/spacecraft interactions. To accomplish these goals, the program involves plume modeling[4,5] and experimental investigations carried out at the NASA John H. Glenn Research Center at Lewis Field (GRC) facilities.[6–8] Our studies initiated with the Lincoln Experimental Satellite (LES) 8/9 PPT and included contamination assessment using quartz crystals, measurements of ion current density using planar langmuir probes, and determination of ion velocity using single langmuir probes.[6] It was found that measurable changes in transmittance of the quartz samples were confined to 30 deg. The centerline ion velocity was estimated at 40 km/s and the ion density at 6×10^{18} m^{-3} at a distance of

24 cm from the thruster. Subsequent investigations of the LES 8/9 plume using time-of-flight analysis of single langmuir probe data found two ion populations, traveling at velocities of approximately 30 and 60 km/s, respectively.[7] The composition of the PPT plume was qualitatively studied using a residual gas analyzer, identifying C, F, C_xF_y, and various thruster materials, similar to results obtained by other investigators.[9–11] Additionally, fast ionization gauges were used and detected the presence of slow neutral particles up to 1 ms after the discharge had ended, indicating an inefficient use of the propellant.[7]

In this investigation triple Langmuir probes are used to simultaneously measure electron temperatures and electron densities in the plume of a laboratory-model PPT. Previous plume investigations of plasma density and temperature have used interferometers and single and double langmuir probes.[12–15] Triple langmuir probes offer many advantages over these methods, allowing simultaneous measurement of electron temperature and density.[16,17] Unlike single and double langmuir probes, the triple langmuir probe does not require a voltage sweep, a task which is difficult in the PPT due to the short-pulse duration. Additionally, triple probes are relatively easy to setup and operate, not requiring the extensive optics of an interferometer. Triple probes have been used successfully in the steady plumes of magnetoplasmadynamic (MPD) thrusters[18,19] and arcjets.[20]

This paper details the application of triple probes in the unsteady (15-μs pulse duration) plume of a rectangular-geometry PPT and expands our preliminary analysis.[8] Probes were attached to a translation table that allowed data collection in the plume on two planes perpendicular and parallel to thruster electrodes passing through the thruster's centerline. Measurements were obtained for radial distances of 6, 10, 12, 14, 16, 18, and 20 cm and for polar angles of 10, 20, 30, and 45 deg with respect to the center of the Teflon® propellant face. The thruster was operated at discharge energy levels of 5, 20, and 40 J. Compared to previous PPT investigations,[12–15] the thruster design used in this work is similar to the one carried on the EO-1 spacecraft, and the energy levels address several planned PPT applications.[3] In this paper the probe construction, grounding scheme, and cleaning procedure are discussed. The data reduction methodology, error analysis, and temperature and density traces are presented and discussed. The spatial variation of the maximum and time-average temperature and density is presented, and the effects of the PPT discharge energy on temperature and density levels are discussed.

Experimental Apparatus

Thruster and Facility

A laboratory-model PPT with a rectangular geometry was used in this study. The PPT is similar to the one flown on the EO-1 spacecraft and was designed at NASA GRC for component life tests and plume characterization. The thruster has 2.5-cm-square electrodes as shown in Fig. 1 and is almost identical in size and performance to the LES 8/9 model with operational characteristics shown in Table 1. Experiments were conducted in a 0.5-m-diam, 1-m-tall bell jar under base pressures between 1×10^{-5} and 5×10^{-5} torr. The thruster was placed at the bottom of the facility, firing upward, with the probes mounted on a vertical translation table that was computer-controlled outside of the tank. This arrangement is shown in Fig. 2. For off-centerline measurements, the thruster was rotated through the appropriate angle, with the probe aligned geometrically with the center of the Teflon face.

Diagnostics and Procedures

The theory of operation of a triple langmuir probe was first outlined by Chen and Sekiguchi in 1965.[16] A symmetric triple langmuir probe, similar to the ones used in our experiments, consists of three identical probes placed in the plasma. One of the probes, indicated as probe 2 in Fig. 3a, is allowed to float in the plasma, and a fixed voltage V_{d3} is applied between the positive and negative with respect to the floating potential probes. The resulting voltage difference $V_{d2}(t)$ and collected current $I_3(t)$ allow the evaluation of $T_e(t)$ and $n_e(t)$ (Refs. 16 and 17) based on a theory that is summarized subsequently.

Table 1 Operational characteristics of the laboratory-model PPT

Discharge energy, J	Impulse bit, μN · s	Mass loss/pulse, μg/pulse	Specific impulse, s
5.3	36	—	—
20.5	256	26.6	982
44.0	684	51.3	1360

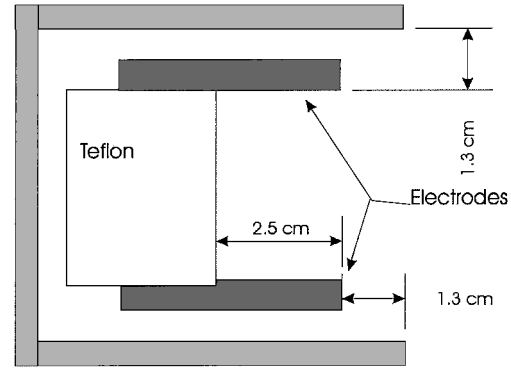

Fig. 1 Schematic of the laboratory-model PPT used in the experiments.

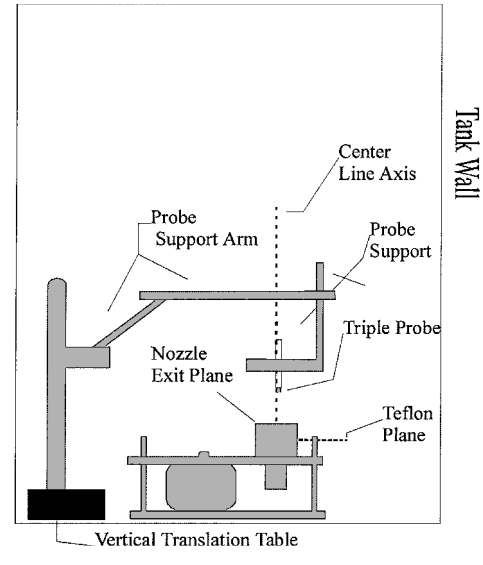

Fig. 2 Experimental apparatus.

For every temporal measurement of $V_{d2}(t)$ and current $I_3(t)$, an initial value of $T_e(t)$ is obtained from the solution of the implicit equation

$$\frac{1}{2} = \frac{1 - \exp(-\chi_{d2})}{1 - \exp(-\chi_{d3})} \tag{1}$$

where $\chi_{d2} = \chi_2 - \chi_1$, $\chi_{d3} = \chi_3 - \chi_1$, and $\chi_n = e|V_n - V_p|/(kT_e)$ is the nondimensional potential at probe $n = 1, 2, 3$ measured with respect to the plasma (or space) potential V_p. This implicit equation is formulated using the thin-sheath current collection model. The electron density is then obtained from

$$n_e = \frac{e^{0.5}(I_3/A_3)}{e(kT_e/m_i)^{0.5}\{1 - \exp[-(\chi_{d3} - \chi_{d2}]\}} \tag{2}$$

With these initial estimates, corrected values for temperature and density can be obtained using improved ion current-collection models. Chen and Sekiguchi[16] and Chen[17] introduced such a model through the equation

$$J_i^2(V) = J_i^2(V_f)[1 + \beta(V - V_f)] \tag{3}$$

where β indicates the variation of ion current as a function of probe potential. This constant can be also written in terms of a nondimensional parameter

$$\eta = \beta\left(\frac{kT_e}{e}\right) = \left(\frac{\mathrm{d}J_i^2(\chi)}{\mathrm{d}\chi}\right)_f \frac{1}{J_i^2(\chi_f)} \tag{4}$$

To derive η, we use the approach by Tilley et al.[18] They combined Eq. (3) with Peterson and Talbot's[21] ion current-collection model

$$J_i(\chi) = J_{i0}(B + a)^a \tag{5}$$

The parameters α and B are obtained from curve-fits to the Laframboise current-collection model

$$\alpha = \frac{2.9}{\ell n(r_p/\lambda_D) + 2.3} + 0.07\left(\frac{T_i}{Z_i T_e}\right)^{0.75} - 0.34 \tag{6}$$

$$B = 1.5 + (T_i/Z_i T_e\left\{0.85 + 0.135[\ell n(r_p/\lambda_D)]^3\right\} \tag{7}$$

The Debye length is

$$\lambda_D = \sqrt{\varepsilon_0 kT_e/e^2 n_e} \tag{8}$$

From Eqs. (3) and (5), η can be evaluated as

$$\eta = 2\alpha/(B + \chi_f) \tag{9}$$

The floating potential χ_f can be derived from the solution of

$$(m_i/m_e)\exp(-2\chi_f) = [B + \chi_f]^{2\alpha} \tag{10}$$

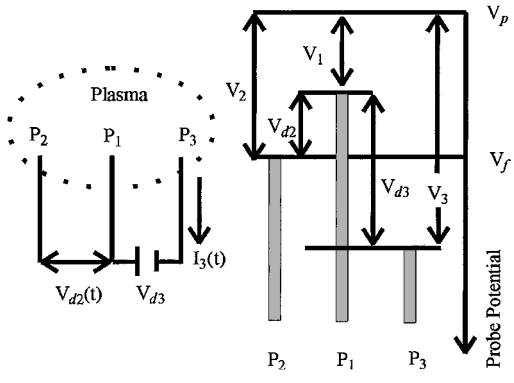

Fig. 3a Triple langmuir probe schematic with potentials at each probe.

The improved implicit equation for the electron temperature is

$$\frac{1}{2} = \frac{1 - 0.5[1 - \beta V_{d2}]^{0.5} + [1 + \beta(V_{d3} - V_{d2})]^{0.5}\exp(-\chi_{d2})}{1 - \exp(-\chi_{d3})} \tag{11}$$

Calculation of the density follows through

$$\eta_e = \frac{\exp(0.5)(I_3/A_3)[1 - \eta(\chi_f - 0.5)]^{0.5}}{e(kT_e/m_i)^{0.5}\{[1 + \eta(\chi_{d3} - \chi_{d2})]^{0.5} - \exp[-(\chi_{d3} - \chi_{d2})]\}} \tag{12}$$

Alternative formulations of triple-probe theory based on improved ion-collection models have been applied to both MPD[18,19] and arcjet thruster[20] plumes with good results.

The electronics diagram in this experiment is shown in Fig. 3b. The applied V_{d3} was supplied by three 9-V batteries in series. In our experiments, the value of V_{d3} was measured after each set of 40 measurements for each angular and 8 radial positions and was found to reduce from 27 V to about 24 V. The V_{d3} was found to reduce by no more than 0.01 V at the end of a set of five measurements at a specific angular and radial position. The V_{d3} was also measured during the pulse and found to reach occasionally a minimum of about 18 V during the peak current of the 40-J discharge. These variations of the applied V_{d3} were accounted for in our data analysis, and it was found that did not affect the evaluation of temperature and density.

Floating voltage probes were attached to probes 1 and 2, and the voltage $V_{d2}(t)$ was found by subtracting the signals digitally on a Lecroy 9314M quad 300-MHz oscilloscope. This method proved to be less susceptible to noise than the use of differential operational amplifiers in previous investigations.[18] A Hall-effect current probe was used to measure $I_3(t)$, and this output was also recorded on the oscilloscope. The probe wires were made of 0.25×10^{-3} m diameter tungsten wire with exposed length of 9×10^{-3} m to minimize end effects, and the average probe spacing was approximately 10^{-3} m.

Implementation of the triple probe in the PPT plume requires careful consideration of plasma and probe parameters that enter in the evaluation of $T_e(t)$ and $n_e(t)$ (Refs. 16–18.) Estimates are obtained assuming that the PPT plume is composed of single-ionized C^+ and F^+ ions with mole fraction $[C^+]/[F^+] = 0.5$, T_e in the range of 2–5 eV, and n_e in the range of 10^{19}–10^{21} m^{-3}. From Table 2 it is evident that the plume plasma is dense ($r_p > \lambda_D$) and that the probes operate for the most part in the collisionless regime ($Kn_{st} = \lambda_{st}/r_p \geq 1$)

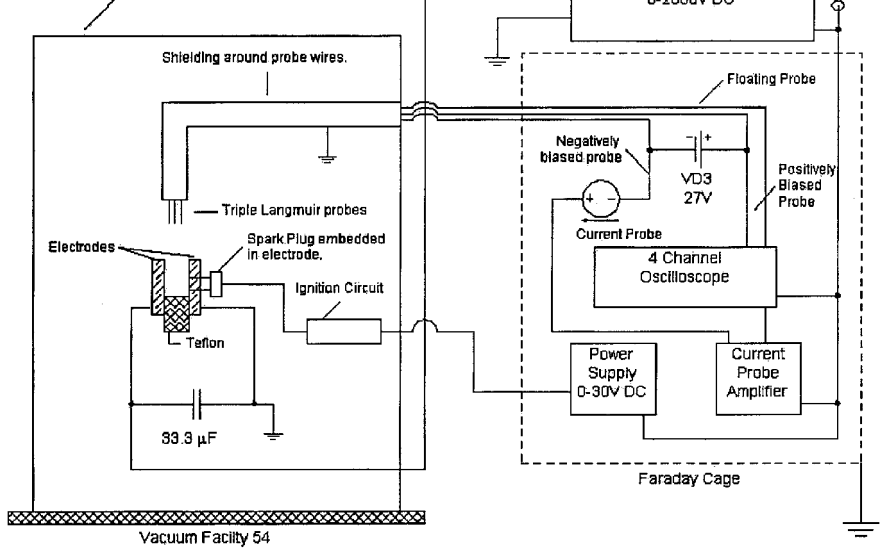

Fig. 3b Electronic circuitry used in the experiments.

Table 2 Parameters related to a triple probe with $r_p = 0.125 \times 10^{-3}$ m, and $s = 10^{-3}$ m operating in a PPT plume[a]

Plasma conditions	Triple probe parameters			
	r_p/λ_D	s/d_s	Kn_{ii}	Kn_{ei}
$n_e = 10^{19}$ m^{-3}, $T_e = 2$ eV	37.6	17.8	4.8	75.9
$n_e = 10^{19}$ m^{-3}, $T_e = 5$ eV	23.7	16.9	4.8	415.2
$n_e = 10^{20}$ m^{-3}, $T_e = 2$ eV	118	42.3	0.58	8.64
$n_e = 10^{20}$ m^{-3}, $T_e = 5$ eV	75.2	40.0	0.58	46.
$n_e = 10^{21}$ m^{-3}, $T_e = 2$ eV	376.1	100.2	0.08	1.
$n_e = 10^{21}$ m^{-3}, $T_e = 5$ eV	237.8	94.4	0.08	5.2

[a]Mole fraction of $[C^+]/[F^+] = 0.5$ and $T_{C+} = T_{F+} = 0.5$ eV.

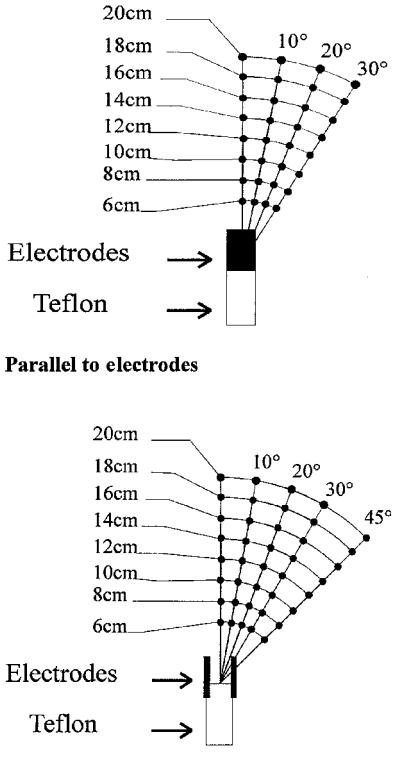

Fig. 4 Triple-probe measurement locations parallel and perpendicular to the electrodes plane passing through the thruster centerline; radial and angular positions are referenced with respect to the center of the Teflon surface.

with little interference due to sheath interactions ($s \gg d_s \geq \lambda_D$). The errors and uncertainty associated with the parameters described in Table 2 as well as other factors are discussed in the error-analysis section that follows.

For each discharge energy level of 5, 20, and 40 J, measurements were taken at eight downstream locations, ranging from 6 to 20 cm from the Teflon surface in 2-cm increments. These measurements were taken at polar angles of 10, 20, and 30 deg on two planes perpendicular and parallel to the electrodes passing through the thruster's centerline. Additionally, measurements were taken at 45 deg off centerline on the plane perpendicular to the thruster electrodes. These locations are shown in Fig. 4. Five pulses were recorded at each spatial location, resulting in a total of 930 data samples. Each sample lasted for 100 μs and included 10,000 voltage and current measurements.

An important consideration in using probes in a plume is possible adverse effects due to probe contamination.[18] After approximately 30–40 pulses, the voltage $V_{d2}(t)$ was found to develop an offset while the probes were covered by a dark deposit. To eliminate this phenomenon, a glow discharge method was implemented where argon gas was fed to the probe-head and an arc was maintained for approximately 10 s between the probe tips and a nearby electrode. It was found that approximately 30–40 pulses could be recorded between each glow discharge cleaning.

Data Reduction and Error Analysis

A typical set of voltage and current trace output from the triple langmuir probes is shown in Fig. 5. Because of the triggering circuit, all pulses begin at 40 μs. Of particular interest in these measurements is the presence of noise. The first source of noise is due to the electromagnetic burst emitted at the start of the pulse as the spark plug initiates the discharge.[22] The second source of noise (indicated in Fig. 5) is due to insufficient oscilloscope resolution of the voltage measurements.

The Loess (locally weighted regression) algorithm is applied to the voltage and current traces, to reduce the noise using a statistical package S-Plus.[23] Loess fits a function about a certain data point using a specified number of neighbors around it. The calculation of the least-squares fit assigns more weight to the points closer to the data point of interest and the implementation of this method in S-Plus allows local residuals to be evaluated. The Loess span is set

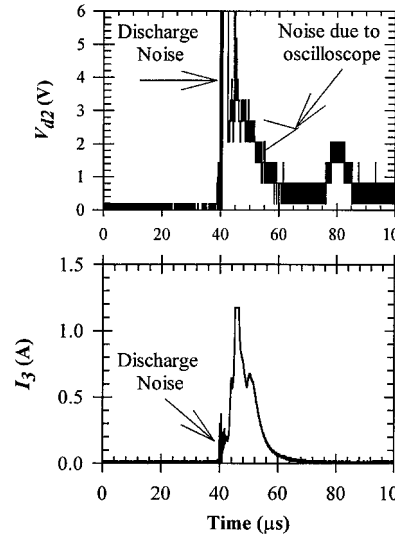

Fig. 5a Voltage and current traces obtained from the triple probe showing various sources of noise.

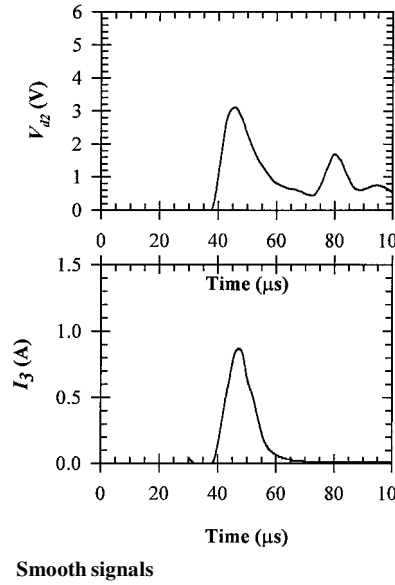

Fig. 5b Same voltage and current traces after data reduction with Loess smoothing.

to 0.2, meaning that 20% of the data is considered for each data point and a second-degree polynomial is generated for each local fit. A typical result is shown in Fig. 5. Using the smoothed voltage and current data are used, electron temperature and density are obtained using the model equations (1–12).

Error Analysis

The uncertainly in measurements of electron temperature using a triple probe is associated with the nondimensional parameter $\eta = \beta(kT_e/e)$ in Eq. (3).[16–18] For values of $\chi_{d3} = e|V_{d3} - V_p|/kT_e \approx 5-10$ the uncertainty is less than 5% and increases weakly for higher values of χ_{d3} (Ref. 18). In our experiment $5.6 \leq \chi_{d3} \leq 28.1$, and we can use the values of Chen,[17] who showed that for $0.02 \leq \eta \leq 0.15$ the uncertainly in electron temperature is smaller than 20%.

The uncertainty in density measurements for $17 \leq r_p/\lambda_D \leq 100$ and $5 \leq \chi_{d3} - \chi_{d2} \leq 25$ is 40–60% assuming that $T_i/Z_iT_e = 1$ (Ref. 18). In the PPT plume, it is expected that $T_i/Z_iT_e < 1$, which will make the uncertainty smaller than the $T_i/Z_iT_e = 1$ case. Note that the Petersen/Talbot[21] curve fit to Laframboise's ion current model used for our data analysis is optimal for $5 \leq r_p/\lambda_D \leq 100$, but higher ratios will still provide a very good estimate.[17,18] For $r_p/\lambda_D \geq 100$, the parameter η is approximately 0.02, and the uncertainty becomes smaller.[17,18]

No sheath interaction is expected in our experiment because $s/d_s \gg 1$ as shown from Table 2. Ion collisions in cases where $Kn_{ii} \leq 1$ account for an increase in ion current of approximately 10–20% (Ref. 18). For $Kn_{ei} > 200/(r_p/\lambda_D)$, a condition met for most cases as values from Table 2 show, the effects of electron collisions on the electron current may be ignored.[18]

The triple probe was aligned with the polar angle measured from the center of the Teflon surface, and this may have resulted in probe misalignment with the flow vector. In fact investigations using a PPT similar to the one used in our experiment showed that the plume is canted toward the cathode by less than 5 deg on the plane perpendicular to the electrodes.[24] Earlier plume studies indicate also a less than 10-deg asymmetry with respect to the geometric centerline of the thruster on the perpendicular plane.[14,25] These studies confirmed that the plume is symmetric on the parallel to the electrodes plane.[14,24–26] Therefore, it is important to assess the impact on the triple-probe output due to the flow/probe misalignment. In MPD thruster plume studies with $n_e \leq 10^{19}$ m^{-3}, $T_e \approx 1-5$ eV, and $r_p/\lambda_D = 18$, it was found that the error due to misalignment was smaller than the experimental uncertainty of the triple probe and that the triple-probe output was insensitive to probe angles of up to 30 deg with respect to the thruster axis.[18] It has also been shown[19] that for $r_p/\lambda_D = 208$ a 5-degree misalignment increases the current by almost 25%. As our Table 2 shows, ratios $r_p/\lambda_D > 100$ occur at the center of the PPT plume, where flow/probe misalignment is less than 5 degrees. Therefore, it is confidently assumed that the effects of misalignment will not adversely affect our measurements, although experimental determination is required to quantify the uncertainty associated with it.

For a probe aligned with the flow, the end-effects are negligible if the parameter $\tau_L = (L_p/\lambda_D)(kT_e/m_i)^{1/2}U_i^{-1} \gg 50$ (Ref. 27). For the plasma conditions listed in Table 2 and when using a maximum ion speed of $U_i \sim 40$ km/s, this parameter is conservatively estimated to be $\tau_L \gg 230$. This further ensures that the ion current is not sensitive to any small misalignments between the probe and the flow vector.

As discussed earlier, the voltage probes and oscilloscope used to record $V_{d2}(t)$ introduced a high-frequency bit error in the temperature measurements with a maximum of ± 0.75 eV occurring at the peak of the pulse. The noise in the current measurements was minimal, and the effect of the voltage noise introduced a $\pm 10\%$ uncertainty into the density measurements.

The spatial resolution of the probes is related to the total volume taken by the probe tip. For our case, the probe volume is cylindrical with a diameter of 2×10^{-3} m and a length of 9×10^{-3} m. All spatial locations reported are measured to the tip of the probe wires. The probe tip was observed to vibrate during testing, due to the backing pump attached to the oil diffusion pump. This vibration was estimated to be approximately $\pm 10^{-2}$ m in each direction, and this distance defines the spatial accuracy of our measurements.

Therefore, for all measurements, the maximum uncertainty in $n_e(r, \theta, t)$ is estimated to be 60%, the maximum uncertainty in $T_e(r, \theta, t)$ is ± 0.75 eV, and the spatial accuracy is within $\pm 10^{-2}$ m.

Data Analysis and Discussion

Electron Temperature and Density

Figure 6 shows typical electron density and electron temperature traces for the 20-J case for $r = 6$, 18, and 18 cm at $\theta_\perp = 10$ deg on the perpendicular plane. The bounding traces are plotted for each location, showing the shot-to-shot variability, as well as the unsteady character of the PPT plume as it passes by the triple probe. Simultaneous electron temperature and density for a 20-J pulse measured at $r = 12$ cm and $\theta_\perp = 10$ deg are plotted in Fig. 7. From Figs. 6 and 7, it is seen that the highest electron temperature for each spatial location occurs at the beginning of the pulse, while the highest density occurs near the middle of the pulse. In some of the electron temperature traces, as shown in Fig. 5, there is a secondary peak after the plasma passes the probe. There is no corresponding density increase at this time, and it was concluded that this peak is due to electrical noise or grounding problems. It should be noted that this is not expected to impact the evaluated data. Because of a consistent experimental error, centerline values are not reported for any of the thruster discharge energy levels.

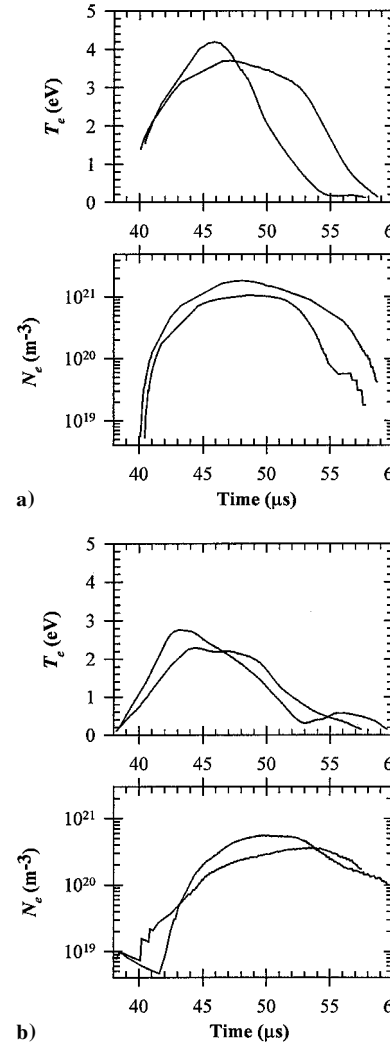

Fig. 6 Bounding temperature and density traces obtained from the triple probe at $\theta_\perp = 10$ deg in a 20-J PPT plume at radial locations of a) $r = 6$ cm and b) $r = 18$ cm.

Table 3 95% Confidence interval for $T_e^*(r,\theta)$ and $N_e^*(r,\theta)$ in the plume of a 5-J PPT

	$\theta_\perp = 10$ deg		$\theta_\perp = 20$ deg		$\theta_\perp = 30$ deg		$\theta_\perp = 45$ deg		$\theta_\parallel = 10$ deg		$\theta_\parallel = 20$ deg		$\theta_\parallel = 30$ deg	
r, cm	T_e^*	N_e^*	T_e^*	N_e^*	T_e^*	N_e^*	T_e^*	N_e^*	T_e^*	N_e^*	T_e^*	N_e^*	T_e^*	N_e^*
6	0.598	9.55E+19	0.274	1.19E+20	0.234	3.25E+19	——	——	0.391	6.45E+19	0.236	3.39E+19	0.275	5.86E+19
8	0.585	1.09E+20	0.261	7.31E+19	0.201	1.18E+19	1.41	3.24E+20	0.262	1.57E+19	0.307	2.67E+19	0.103	1.69E+19
10	0.948	3.27E+19	0.313	6.02E+19	0.382	3.49E+19	1.43	1.96E+19	0.232	1.16E+19	0.441	2.94E+19	0.065	7.29E+18
12	0.417	2.00E+19	0.916	4.20E+19	0.467	9.03E+18	0.301	6.67E+18	0.315	1.48E+19	0.785	7.40E+18	0.593	5.75E+18
14	0.22	1.36E+19	1.03	4.41E+19	0.436	7.01E+18	0.566	1.20E+19	0.403	3.96E+19	0.409	4.30E+18	0.651	6.00E+18
16	1.16	1.16E+19	0.355	1.59E+19	0.201	7.71E+18	0.548	7.38E+18	0.76	6.13E+18	0.432	9.80E+17	0.334	3.56E+18
18	0.698	8.28E+18	0.371	6.83E+18	0.617	9.71E+18	0.498	1.56E+19	0.376	6.05E+18	0.49	5.58E+18	0.292	2.01E+18
20	1.27	9.18E+18	2.07	6.86E+18	0.682	4.27E+18	1.29	9.60E+18	0.57	2.38E+18	0.31	4.30E+18	0.909	3.99E+18

Table 4 95% Confidence interval for $T_e^*(r,\theta)$ and $N_e^*(r,\theta)$ in the plume of a 20-J PPT

	$\theta_\perp = 10$ deg		$\theta_\perp = 20$ deg		$\theta_\perp = 30$ deg		$\theta_\perp = 45$ deg		$\theta_\parallel = 10$ deg		$\theta_\parallel = 20$ deg		$\theta_\parallel = 30$ deg	
r, cm	T_e^*	N_e^*	T_e^*	N_e^*	T_e^*	N_e^*	T_e^*	N_e^*	T_e^*	N_e^*	T_e^*	N_e^*	T_e^*	N_e^*
6	0.938	3.16E+20	0.376	4.37E+20	0.66	2.68E+20	—-	——-	0.524	2.54E+20	1.2	3.47E+20	0.4	1.23E+20
8	0.529	4.19E+20	0.308	2.16E+20	0.451	3.25E+20	0.462	1.33E+20	0.226	1.46E+20	0.412	3.68E+20	0.156	1.78E+20
10	0.454	1.65E+20	0.306	2.28E+20	0.542	5.35E+19	0.223	8.50E+19	0.174	4.73E+20	0.356	2.46E+20	0.393	3.04E+20
12	0.696	1.26E+20	0.258	2.01E+20	0.659	6.86E+19	0.696	9.03E+19	0.21	1.31E+20	0.583	2.93E+20	0.409	1.84E+20
14	0.574	2.17E+20	0.392	1.98E+20	0.17	1.49E+20	0.528	1.23E+20	0.287	8.56E+19	0.498	6.32E+19	0.153	1.77E+20
16	0.715	7.76E+19	0.333	5.87E+19	0.185	4.11E+19	0.378	9.41E+19	0.203	1.65E+20	0.364	6.75E+19	0.534	1.38E+20
18	0.431	1.02E+20	0.125	6.13E+19	0.972	7.98E+19	0.622	1.49E+20	0.278	1.95E+20	0.252	8.43E+19	0.167	5.50E+19
20	0.524	1.25E+20	0.594	1.38E+20	1.17	6.49E+19	0.874	6.80E+19	0.435	5.41E+19	0.218	4.36E+19	0.7	4.73E+19

Table 5 95% Confidence interval for $T_e^*(r,\theta)$ and $N_e^*(r,\theta)$ in the plume of a 40-J PPT

	$\theta_\perp = 10$ deg		$\theta_\perp = 20$ deg		$\theta_\perp = 30$ deg		$\theta_\perp = 45$ deg		$\theta_\parallel = 10$ deg		$\theta_\parallel = 20$ deg		$\theta_\parallel = 30$ deg	
r, cm	T_e^*	N_e^*	T_e^*	N_e^*	T_e^*	N_e^*	T_e^*	N_e^*	T_e^*	N_e^*	T_e^*	N_e^*	T_e^*	N_e^*
6	0.75	4.26E+20	1.17	5.11E+20	0.156	3.91E+20	—-	—–	0.324	6.97E+20	0.215	5.09E+20	0.375	4.64E+20
8	0.268	2.99E+20	0.685	1.02E+21	0.293	1.24E+20	0.884	1.60E+20	0.223	2.05E+20	0.247	4.20E+20	0.305	2.30E+20
10	0.977	6.49E+20	0.921	2.70E+20	0.146	9.81E+19	0.778	9.23E+19	0.518	3.96E+20	0.412	4.89E+20	0.231	2.00E+20
12	0.474	3.71E+20	0.569	8.55E+19	1.1	1.99E+20	0.587	1.35E+20	0.237	2.94E+20	0.536	1.99E+20	0.491	3.84E+20
14	0.609	2.80E+20	0.439	1.31E+20	0.698	1.18E+20	0.714	6.57E+19	0.279	2.04E+20	0.089	2.86E+20	0.383	1.23E+20
16	0.833	3.33E+20	0.301	1.30E+20	0.386	9.42E+19	0.707	6.68E+19	0.568	3.70E+20	0.234	2.29E+20	0.501	2.12E+20
18	0.714	2.91E+20	0.548	2.36E+20	0.653	8.15E+19	0.124	6.11E+19	0.423	2.14E+20	0.341	1.55E+20	0.149	1.21E+20
20	0.702	1.91E+20	0.42	1.40E+20	0.157	1.30E+20	0.169	3.88E+19	0.213	5.92E+19	0.273	5.44E+20	0.406	8.74E+19

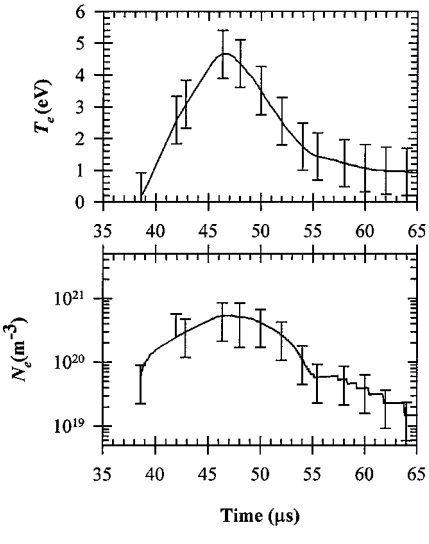

Fig. 7 Simultaneous electron temperature and density for a 20-J pulse measured $r = 12$ cm and $\theta_\perp = 10$ deg showing the earlier arrival of the maximum temperature; maximum uncertainty $N_e(\pm 60\%)$ and $T_e(\pm 0.75$ eV) is also included.

Average Maximum Electron Temperature and Density

To evaluate spatial trends in the expansion of the PPT plume, it is convenient to concentrate our analysis on maximum electron density and temperature measured at each location. In the spatial analysis of the data, the maximum density and temperature for a single trace is recorded at a location (r, θ). These maxima are averaged as

$$T_e^*(r,\theta) = \sum_{i=1,N} T_e^{\max}(r,\theta;i) \Big/ N \tag{13}$$

$$N_e^*(r,\theta) = \sum_{N} n_e^{\max}(r,\theta) \Big/ N \tag{14}$$

where i designates the sample and $N = 5$ designates the number of samples recorded at each location. The error in $n_e^{\max}(r,\theta;i)$ is $\pm 60\%$ and in $T_e^{\max}(r,\theta;i)$ ± 0.75 eV, as discussed earlier. To account for the pulse-to-pulse variation in $n_e^{\max}(r,\theta;i)$ and $T_e^{\max}(r,\theta;i)$, the 95% confidence interval of these maximum values is obtained, and results are shown in Tables 3–5.

Figures 8, 9, and 10 show the spatial variation of plume properties for a 5-, 20-, and 40-J PPT discharge, respectively. Figures 8–10 show some overall similar trends. The average maximum density decreases with increasing distance in both the parallel and perpendicular planes. The average maximum density is larger near the exit and decreases slightly as the plasmoid expands with an angular

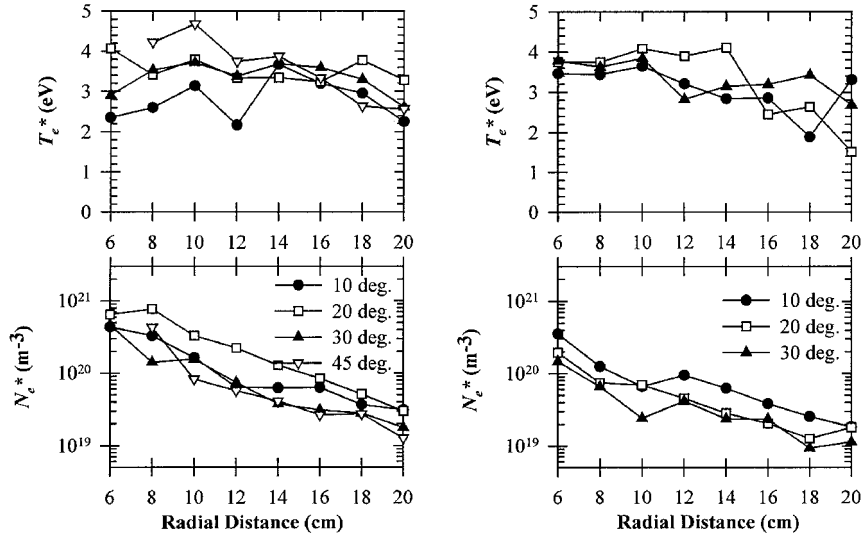

a) Perpendicular plane b) Parallel plane

Fig. 8 Spatial variation of $N_e^*(\pm 60\%)$ and $T_e^*(\pm 0.75$ eV) in the plume of a 5-J PPT.

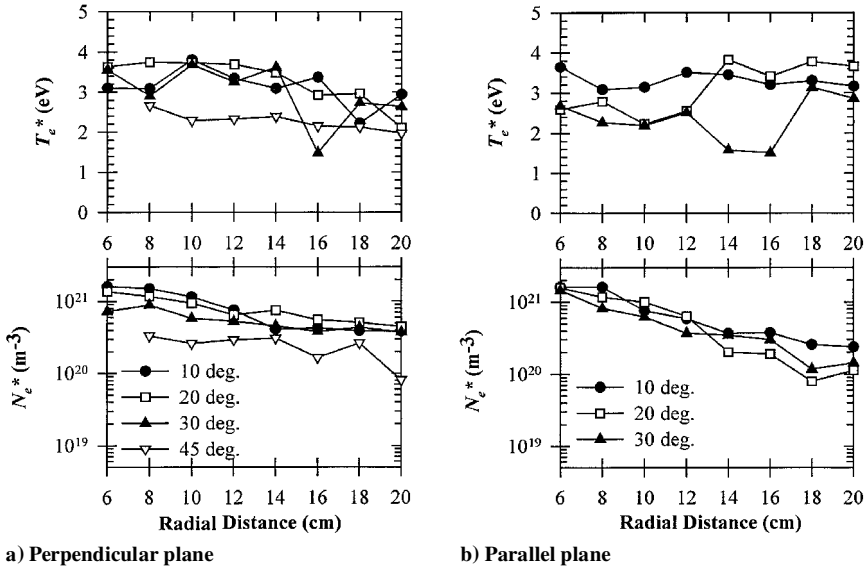

a) Perpendicular plane b) Parallel plane

Fig. 9 Spatial variation of $N_e^*(\pm 60\%)$ and $T_e^*(\pm 0.75$ eV) in the plume of a 20-J PPT.

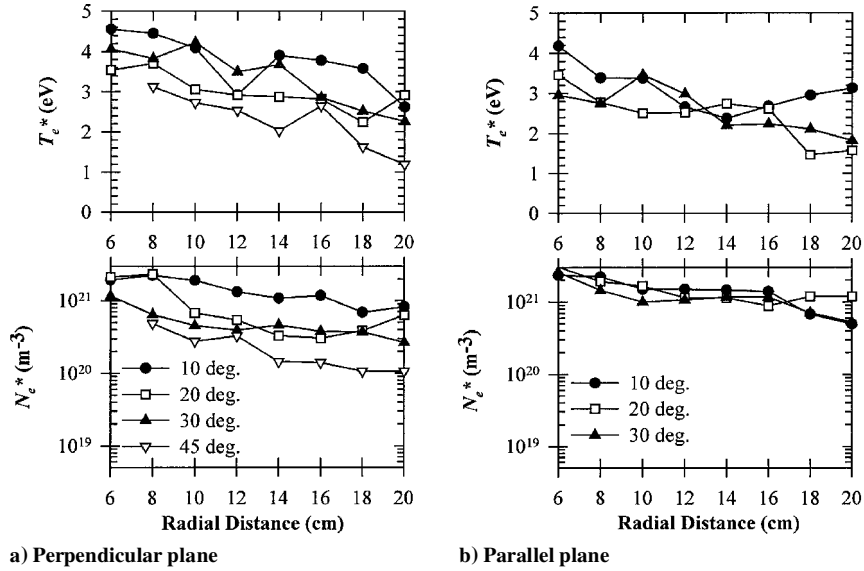

a) Perpendicular plane b) Parallel plane

Fig. 10 Spatial variation of $N_e^*(\pm 60\%)$ and $T_e^*(\pm 0.75$ eV) in the plume of a 40-J PPT.

variation that is also shown in Figs. 8–10. The perpendicular plane shows considerable angular variation in both N_e^* and T_e^*. Figure 9a shows that for the 20-J case N_e^* decreases monotonically with increasing angular position for most part of the plume. At radial distances larger than 12 cm, the values of N_e^* are within the uncertainty for all angles considered. Figures 8b, 9b, and 10b show that there is no considerable variation in N_e^* or T_e^* on the parallel plane. This is direct result of the rectangular electrode configuration of the PPT. T_e^* values are between 2 and 4.5 eV for all energy levels considered.

Time-Average Electron Temperature and Density

The time-average electron temperature $\langle T_e \rangle$ for a location (r, θ) over the duration of the pulse is obtained as

$$\langle T_e \rangle(r,\theta) = \left[\sum_{i=1,N} \left\{ \int_0^P T_e(r,\theta,t;i)\,\mathrm{d}t \right\} \Big/ P \right] \Big/ N \qquad (15)$$

where $N = 5$. Similarly, the time-average electron density is given by

$$\langle N_e \rangle(r,\theta) = \left[\sum_{i=1,N} \left\{ \int_0^P N_e(r,\theta,t;i)\,\mathrm{d}t \right\} \Big/ P \right] \Big/ N \qquad (16)$$

Figures 11, 12, and 13 show the time-average plume properties for a 5-, 20-, and 40-J PPT discharge, respectively. As expected, these plots follow the same trends as the maximum values. The time-average density drops by almost an order of magnitude within a radial distance of 12 cm downstream the PPT exit. The measurements show particularly well the large angular variation of density in the perpendicular plane and the high degree of uniformity in the parallel plane.

For all cases considered, the time-average electron temperature is approximately 3 eV at 6 cm and decreases to about 1 eV at 20 cm from the Teflon surface. These magnitudes compare with recent spectroscopic measurements in a PPT plume.[9] Unlike the time-average density, there is no apparent difference in the time-average temperature between the parallel and perpendicular planes.

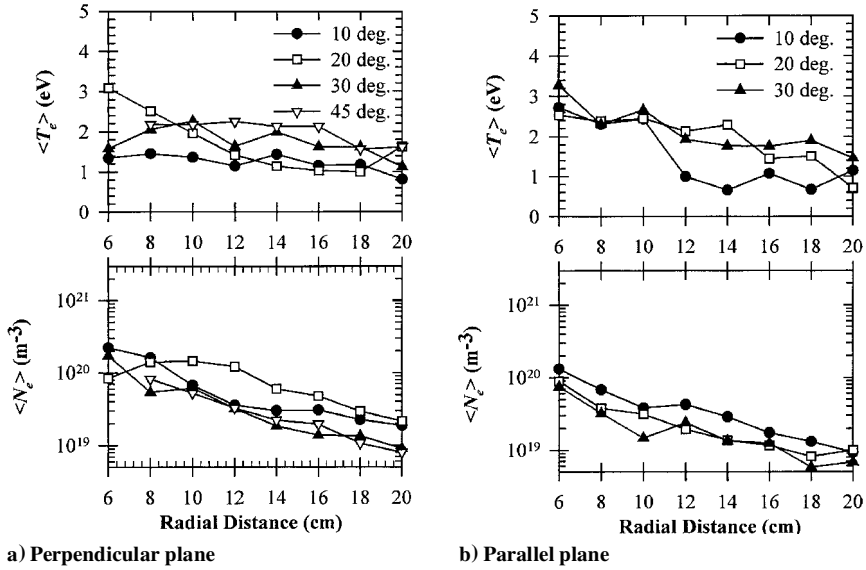

a) Perpendicular plane b) Parallel plane

Fig. 11 Spatial variation of $\langle N_e \rangle$ (± 60%) and $\langle T_e \rangle$ (± 0.75 eV) in the plume of a 5-J PPT.

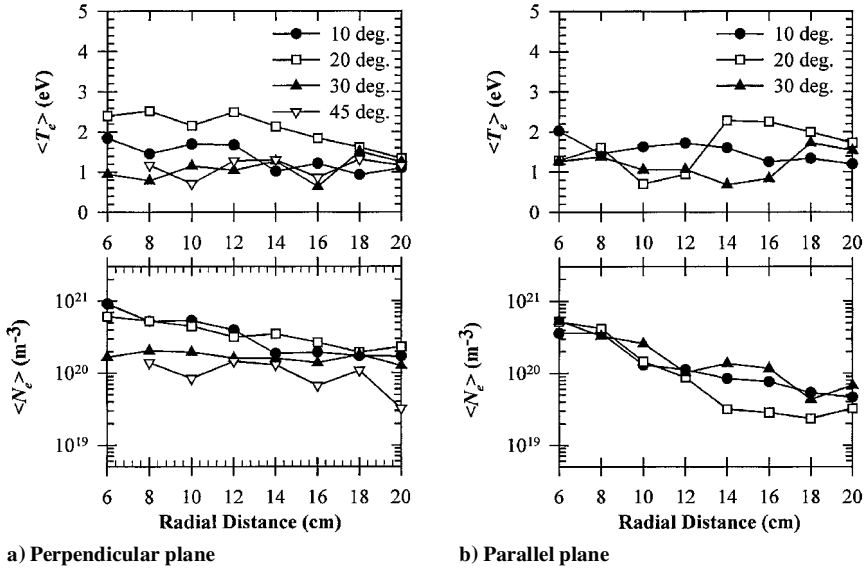

a) Perpendicular plane b) Parallel plane

Fig. 12 Spatial variation of $\langle N_e \rangle$ (± 60%) and $\langle T_e \rangle$ (± 0.75 eV) in the plume of a 20-J PPT.

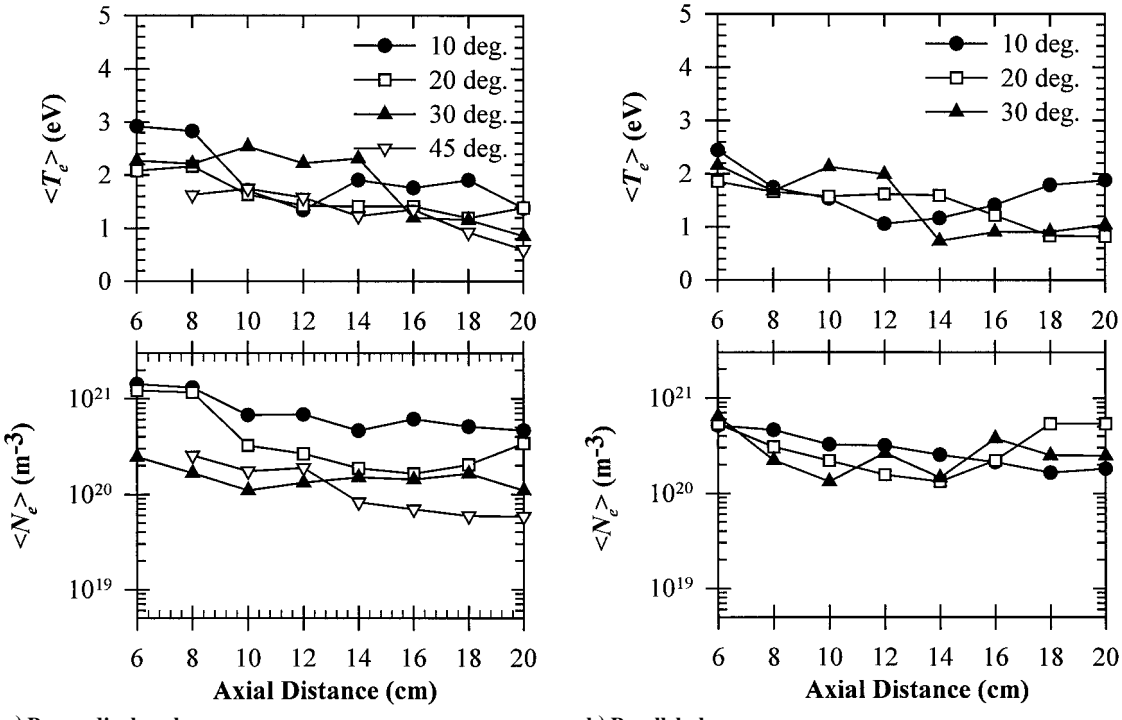

Fig. 13 Spatial variation of $\langle N_e \rangle$ ($\pm 60\%$) and $\langle T_e \rangle$ (± 0.75 eV) in the plume of a 40-J PPT.

Finally, from these data it can be concluded that an increase in the discharge energy results in larger time-average electron densities for all plume locations. The time-average electron temperature, however, remains unaffected within the accuracy of our measurements. These effects should be reexamined with higher fidelity measurements.

Conclusions

The experimental characterization of the plume of a PPT was performed as part of a program that aims in developing an understanding of PPT plume/spacecraft interactions. The experimental setup included triple langmuir probes mounted on a movable probe stand, to collect data over a wide range of locations and operating conditions. The implementation of this measuring technique is discussed in detail, to aid future work that utilizes these devices. The laboratory-model PPT used is a rectangular geometry built for component lifetime tests and plume studies. Electron temperature and density was measured from up to 45 deg from the centerline on planes parallel and perpendicular to the thruster electrodes, for thruster energy levels of 5, 20, and 40 J. Radial distances extend from 6 to 20 cm downstream from the Teflon surface. These locations cover the core of the PPT plume, over a range of energy levels that corresponds to proposed mission operating conditions.[3]

Data analysis shows the spatial and temporal variation of the plume. Maximum electron density near the exit of the thruster is 1.6×10^{20}, 1.6×10^{21}, and 1.8×10^{21} m^{-3} for the 5-, 20-, and 40-J discharges respectively. At 20 cm downstream from the Teflon surface, densities are 1×10^{19}, 1.5×10^{20}, and 4.2×10^{20} for the 5-, 20-, and 40-J discharges, respectively. The maximum electron temperature was found in the range between 3.5 and 4.5 eV at the thruster exit and between 2 and 3.5 eV at 20 cm from the Teflon surface for all discharge energies considered.

The time-average electron density and temperature were also evaluated and found to decrease with increasing radial distance from the Teflon surface. Time-average temperatures are between 1 and 3 eV for all discharge energy levels considered. Time-average electron density increases with increasing discharge energy and range between 10^{19} and 2×10^{20} m^{-3} for the 5-J case, 3×10^{19} and 9×10^{20} m^{-3} for the 20-J case, and 5×10^{19} and 1.4×10^{21} m^{-3} for the 40-J case. For all energy levels considered, plume properties show larger angular variation on the perpendicular plane than the parallel plane. This can be attributed to the rectangular geometry of the PPT electrodes. These measurements confirm the nonsymmetric nature of the PPT plume, which is an important consideration in plume/spacecraft interaction studies. Finally, the measurements show that the increase of discharge energy results in higher electron densities but not temperature.

Acknowledgments

This work was funded in part by NASA Grant NAG3-1873. We gratefully acknowledge Fellowship support for R. Eckman and L. Byrne by the Massachusetts Space Grant Consortium. The authors would like to gratefully acknowledge the assistance of Hani Kamhawi of Ohio State University for his many useful suggestions during the course of the experiment.

References

[1] Guman, W. J., and Nathanson, D. M., "Pulsed Plasma Microthruster Propulsion System for Synchronous Orbit Satellite," *Journal of Spacecraft and Rockets*, Vol. 7, No. 4, 1970, p. 409.

[2] Brill, Y., Eisner, A., and Osborn, L., "The Flight Application of a Pulsed Plasma Microthruster: The NOVA Satellite," AIAA Paper 82-1956, Nov. 1982.

[3] Myers, R. M., Oleson, S., McGuire, M., Meckel, N., and Cassady, R. J., "Pulsed Plasma Thruster Technology for Small Satellite Missions," NASA CR 198427, Nov. 1995.

[4] Gatsonis, N. A., and Yin, X., "Particle/Fluid Modeling of Pulsed Plasma Thruster Plumes," AIAA Paper 99-2299, June 1999.

[5] Yin, X., and Gatsonis, N. A., "Numerical Investigations of PPT Plumes," International Electric Propulsion Conf., IEPC Rept. 97-036, Aug. 1997.

[6] Myers, R. M., Arrington, L. A., Pencil, E. J., Carter, J., Heminger, J., and Gatsonis, N. A., "Pulsed Plasma Thruster Contamination," AIAA Paper 96-2729, July 1996.

[7] Eckman, R., Gatsonis, N. A., Myers, R. M., and Pencil, E., "Experimental Investigation of the LES-8/9 Pulsed Plasma Thruster Plume," *Proceedings of the 25th International Electric Propulsion Conference*, IEPC-97-126, Cleveland, Aug. 1977.

[8] Eckman, R., Byrne, L., Cameron, E., Gatsonis, N. A., and Pencil, E., "Triple Langmuir Probe Measurements in the Plume of a Pulsed Plasma Thruster," AIAA Paper 98-3806, July 1998.

[9] Hirata, M., and Murakami, H., "Exhaust Gas Analysis of a Pulsed Plasma Engine," International Electric Propulsion Conf., IEPC Rept. 84-52, 1984.

[10]Spanjers, G. G., Lotspeich, J. A., and Spores, R. A., "Propellant Losses Because of Particulate Emission in a Pulsed Plasma Thruster," *Journal of Propulsion and Power*, Vol. 14, No. 4, 1998, p. 554.

[11]Markusic, T. E., and Spores, R. A., "Spectroscopic Emission Measurements of a Pulsed Plasma Thruster Plume," AIAA Paper 97-2924, July 1997.

[12]Antropov, N., Gomilka, L., Diakonov, G., Krivonosov, I., Popov, G., and Orlov, M., "Parameters of Plasmoids Injected by PPT," AIAA Paper 97-2921, July 1997.

[13]Thomassen, K. I., and Tong, G., "Interferometric Density Measurements in the Arc of a Pulsed Plasma Thruster," *Journal of Spacecraft and Rockets*, Vol. 10, No. 3, 1973, pp. 163, 164.

[14]Guman, W. J., and Begun, M., "Exhaust Plume Studies of a Pulsed Plasma Thruster," AIAA Paper 97-704, April 1978.

[15]Vondra, R. J., Thomassen, K., and Solbes, A., "Analysis of Solid Teflon Pulsed Plasma Thruster," *Journal of Spacecraft and Rockets*, Vol. 7, No. 12, 1970, pp. 1402–1406.

[16]Chen, S., and Sekiguchi, T., "Instantaneous Direct-Display System of Plasma Parameters by Means of Triple Probe," *Journal of Applied Physics*, Vol. 26, No. 8, 1965, pp. 2363–2375.

[17]Chen, S., "Studies of the Effect on Ion Current on Instantaneous Triple-Probe Measurements," *Journal of Applied Physics*, Vol. 42, No. 1, 1971, pp. 406–412.

[18]Tilley, D. L., Kelly, A. J., and Jahn, R. G., "The Application of the Triple Probe Method to MPD Thruster Plumes," AIAA Paper 90-2667, July 1990.

[19]Gallimore, A. D., Kell, A. J., and Jahn, R. G., "Anode Power Deposition in Quasi-Steady MPD Thusters," AIAA Paper 90-2668, July 1990.

[20]Bufton, S. A., Burton, R. L., and Krier, H., "Measured Plasma Properties at the Exit Plane of a 1-kW Arcjet," AIAA Paper 95-3066, July 1995.

[21]Petersen, E. W., and Talbot, L., "Collisionless Electrostatic Single-Probe and Double-Probe Measurements," *AIAA Journal*, Vol. 8, No. 12, 1970, pp. 2215–2219.

[22]Thomassen, K. I., "Radiation from Pulsed Electric Thrusters," *Journal of Spacecraft and Rockets*, Vol. 10, No. 10, 1973, pp. 679, 680.

[23]*S-Plus 200 Guide to Statistics*, Vol. 1, Data Analysis Products Div., MathSoft, Seattle, WA.

[24]Arrington, L. A., and Haag, T. W., "Multi-Axis Thrust Measurement of the EO-1 PPT," AIAA Paper 99-2290, June 1999.

[25]Rudolph, L. K., Harsatd, Pless, L. C., Jones, R. M., "Plume Characterization of a One-Millipound Solid Teflon Pulsed Plasma Thruster," U.S. Air Force Research Lab., AFRL TR 79-60, Sept. 1979.

[26]Arrington, L. A., Marrese, C. M., and Blandino, J. J., "Pulsed Plasma Thruster Plume Study: Symmetry and Impact on Spacecraft Surfaces," AIAA Paper 2000-3262, July 2000.

[27]Chung, P. M., Talbot, L., and Touryan, K. L., *Electric Probes in Stationary and Flowing Plasmas*, Vol. 2, Springer-Verlag, New York, 1975, pp. 29–32.